ELECTRONIC SUPPLEMENTAL INFORMATION
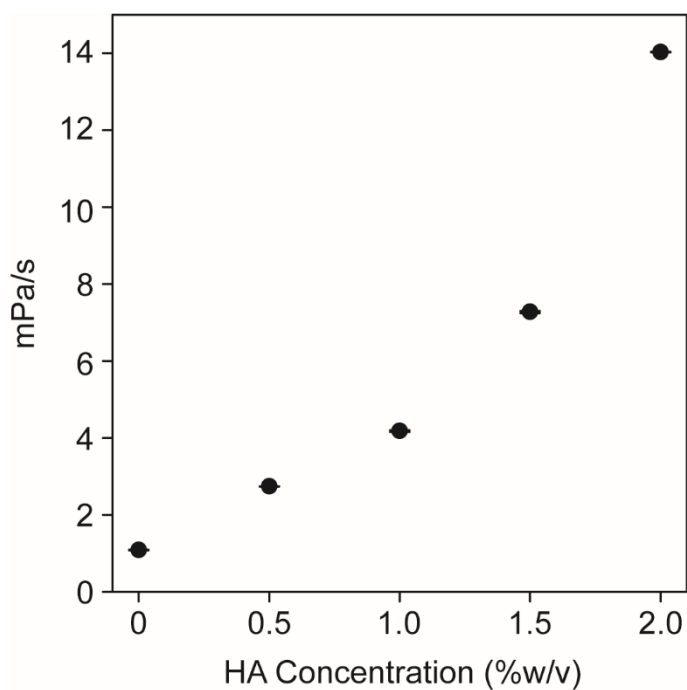
Supplemental Figure 1, HA solution viscosity as a function of concentration. The viscosity of the HA solution prior to gelation is within the range of solution viscosities that can be dispensed using customary liquid handling approaches.
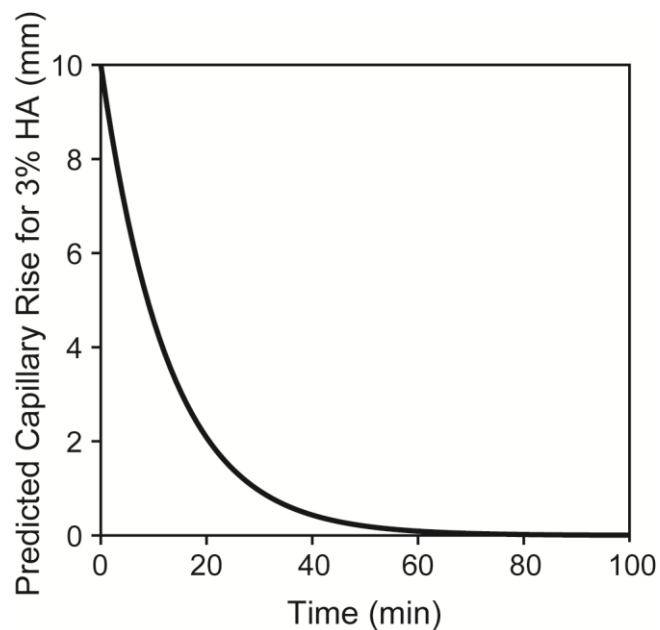
Supplemental Figure 2, Predicted gelation curve for a 3% w/v HA hydrogel synthesized using the reduced reaction volume protocol with added glutathione. Since the thiol-modified HA was too viscous to handle above 2% w/v, the gelation time constant for a 3% w/v gel was extrapolated from the time constant power law (figure 2B) and used to predict the gelation behaviour as it would be observed using the capillary method by Xu et al.[70] The 3% w/v gel would require 40-60 minutes to gel, compared to the 15 minute gelation reported by Shu et al.[33] suggesting that the added glutathione is working to slow down gelation of the material.
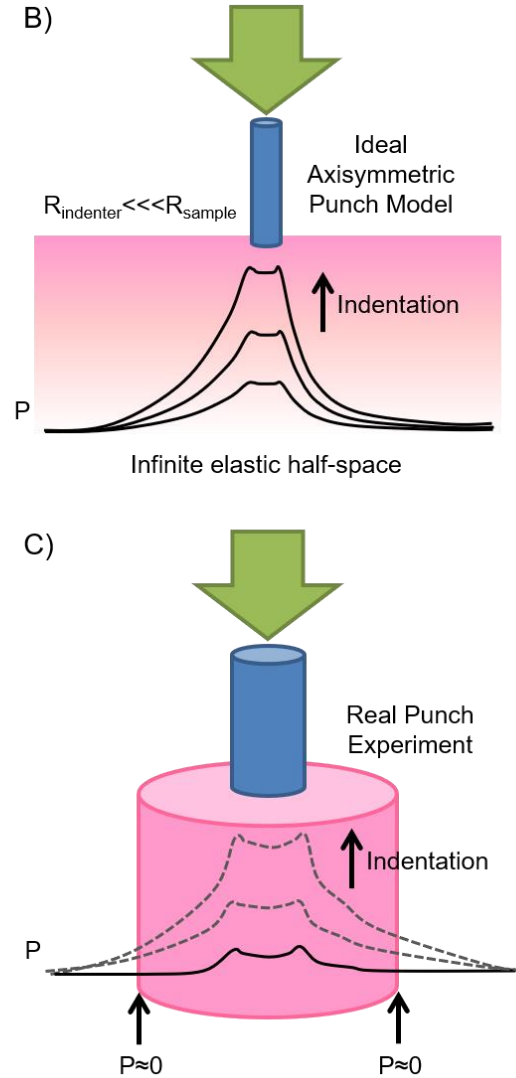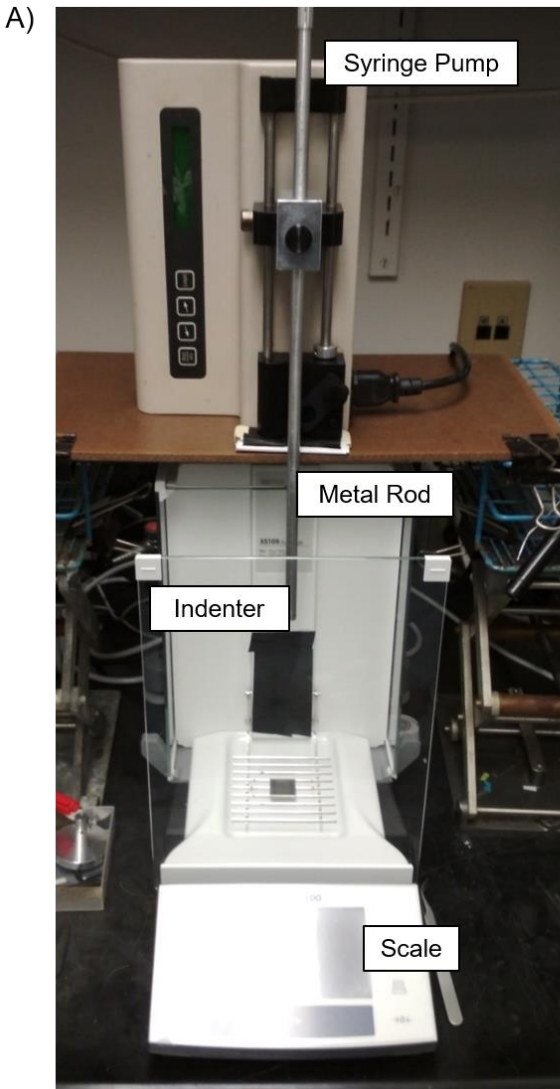
Supplemental Figure 3, Experimental setup for compression testing. A) Compression testing was performed with a modified apparatus originally described by Xu et al.[71] An indenter probe was loaded onto a syringe pump pressing down at constant speed into the HA hydrogel sample contained within a custom 3D printed holder on an analytical balance. The mass reading on the balance was converted to a force measurement and the data were used to plot force versus deformation, which was used to calculate the elastic modulus. **B)** An illustration of the ideal case for Timoshenko and Goodier's contact mechanics model, showing the change in the pressure distribution in the elastic half-space in response to increasing deformation by the indenter. The ideal case is valid for $R_{indentor} <<< R_{sample}$, i.e., a small probe onto an infinite elastic half-space. **C)** In a real contact mechanics case where R_{sample} is not infinite, limits must be set to ensure the experiment does not deviate too much from the ideal case. Deformation was limited to 5%. By limiting deformation, the pressure distribution created by the indenter is negligible before reaching the edge of the sample, thus rendering R_{sample} effectively infinite with respect to the pressure distribution.
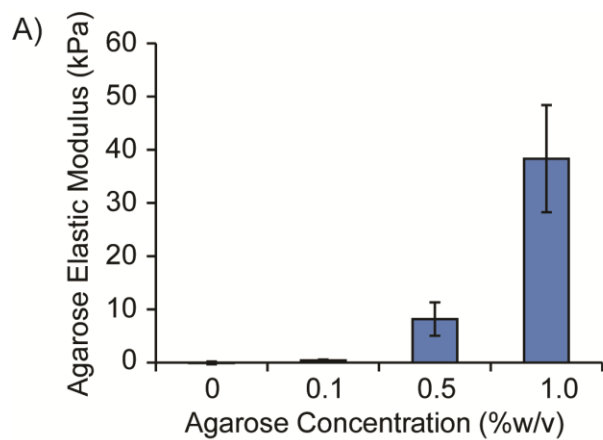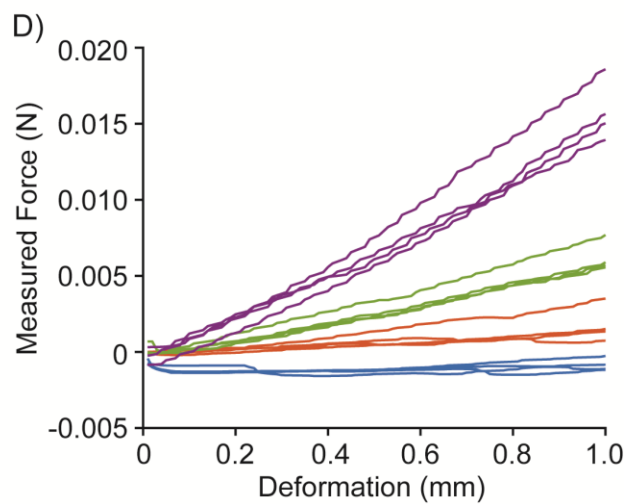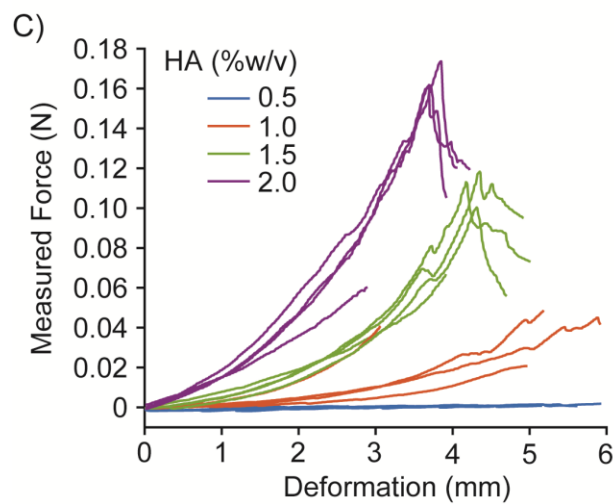
Supplemental Figure 4, Compression testing data. A) The compression test setup was calibrated with agarose gels (and a liquid PBS control), the data for which is presented here graphically and in table form in **(B)**. **C)** Data collected from compression testing of HA hydrogels shows nonlinear behaviour, which is expected of viscoelastic materials. **D)** 'Toe regimes' present at deformations up to 5% or 0.75mm were used to determine the elastic moduli of hydrogel samples.
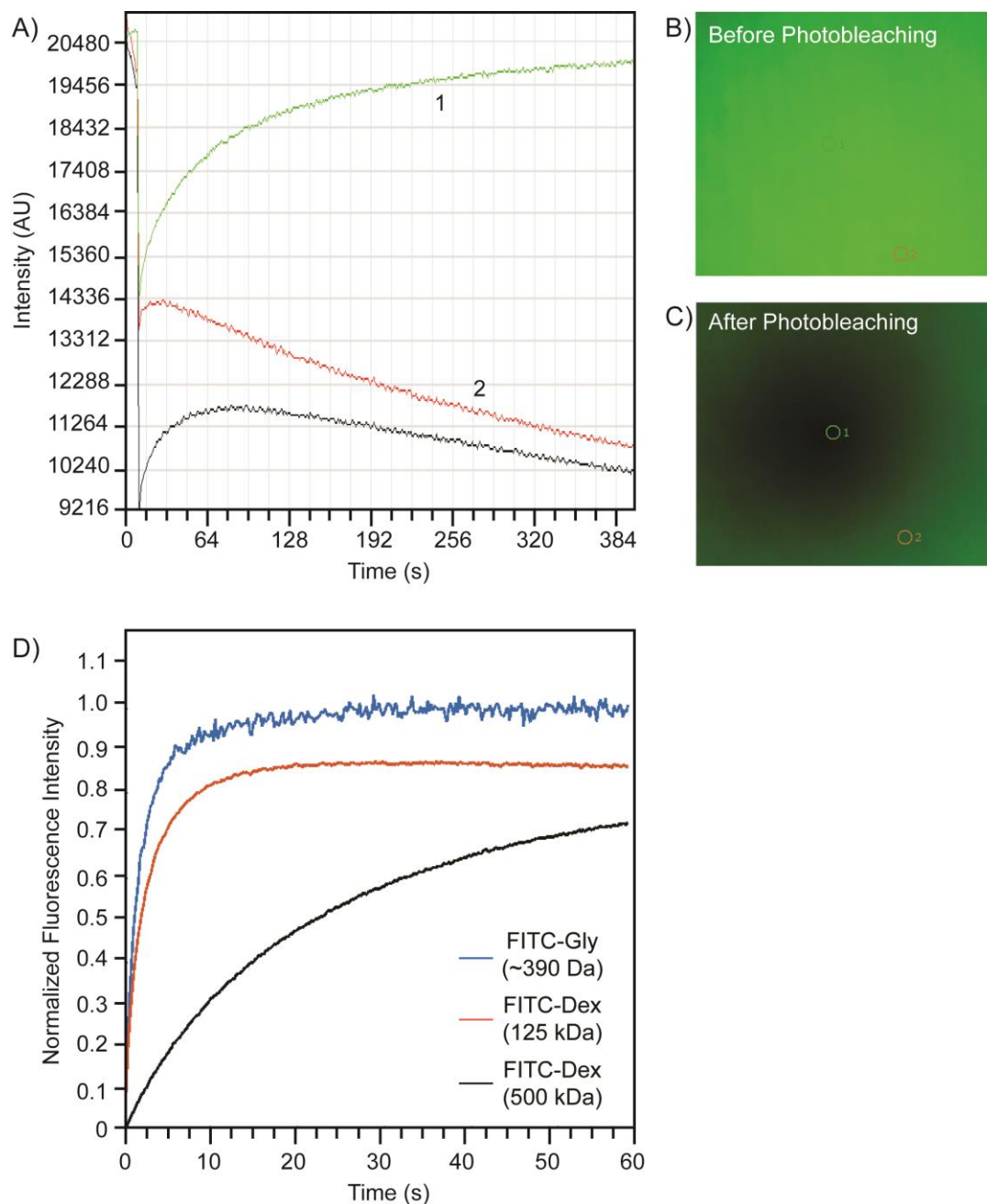
Supplemental Figure 5, Fluorescence recovery after photobleaching. A) Representative data obtained from a FRAP experiment. Curve 1 is obtained from the bleached region of interest and curve 2 is obtained from a reference region outside of the bleach spot. The corrected curve in black is calculated by subtracting the reference curve from the ROI curve. **B)** Representative image of a sample (2% w/v HA hydrogel with 125 kDa FITC-Dex) prior to bleaching. **C)** Image of the same sample immediately after bleaching with the bleach spot centred on the region of interest, labeled as the green circle #1. The red circle #2 is the reference point used for correcting the data. **D)** Representative FRaP curves obtained from different dye particle sizes for a 1% HA hydrogel, normalized (as shown in **(A)**) and plotted together for comparison.
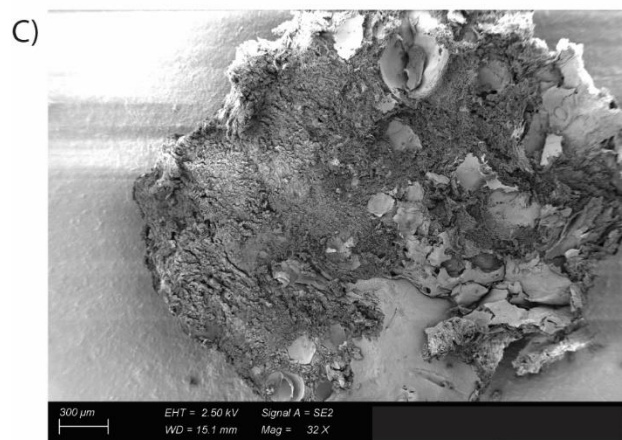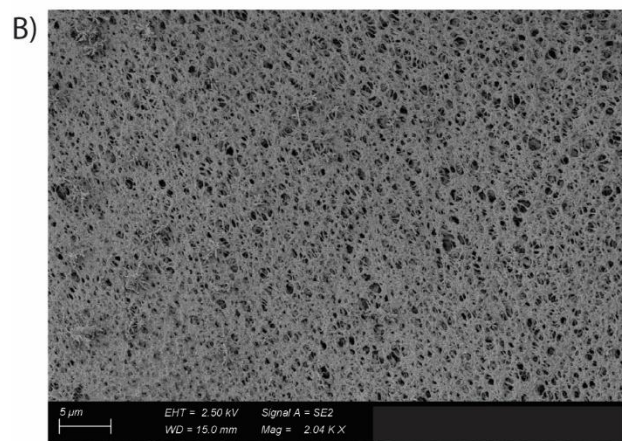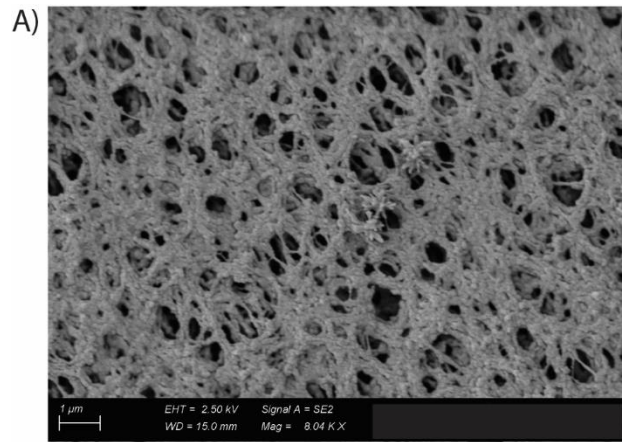
Supplemental Figure 6, Scanning electron microscopy images of HA hydrogel pore structure.
Representative scanning electron microscopy images of **A)** the microporous structure of a 2% HA hydrogel at 8,000X magnification showing a microfibrous structure with an average pore size of 0.023 μm^2 (+/- 0.012 μm^2 standard deviation), **B)** the microporous structure of a 2% HA hydrogel at 2,000X magnification (the approximate length scale over which a single cell would be expected to interact with the material), and **C)** the structure of a 2% HA hydrogel at 32X magnification.
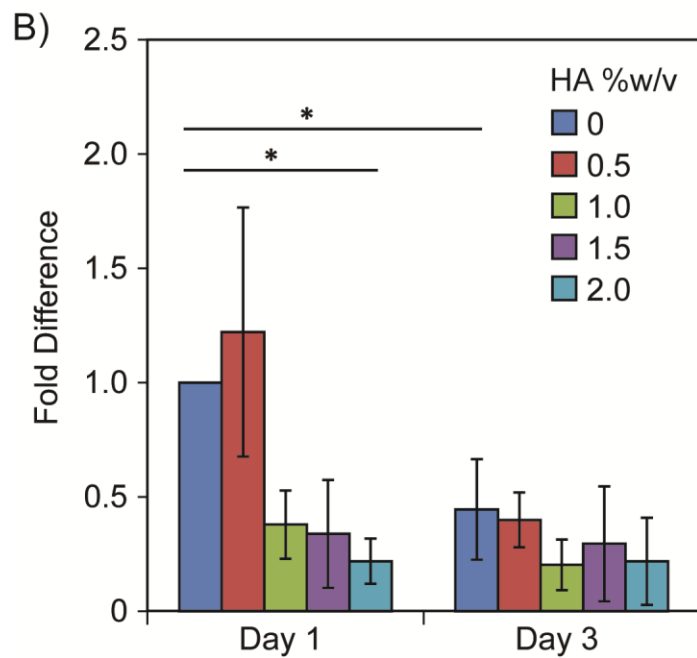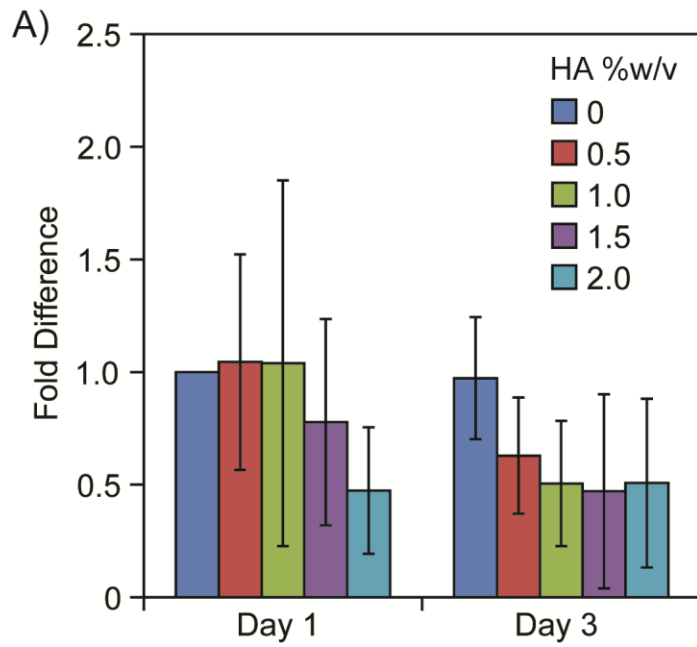
Supplemental Figure 7, ATP content in cells culture beneath HA hydrogels. LNCaP cells **(A)** and PC3 cells **(B)** displayed decreasing ATP levels over 3 days of culture for increasing HA hydrogel content. Significant differences across HA hydrogel concentrations were present for PC3 cells but not LNCaP cells by two-way ANOVA, as indicated by * ($p < 0.05$). Error bars show standard deviation.
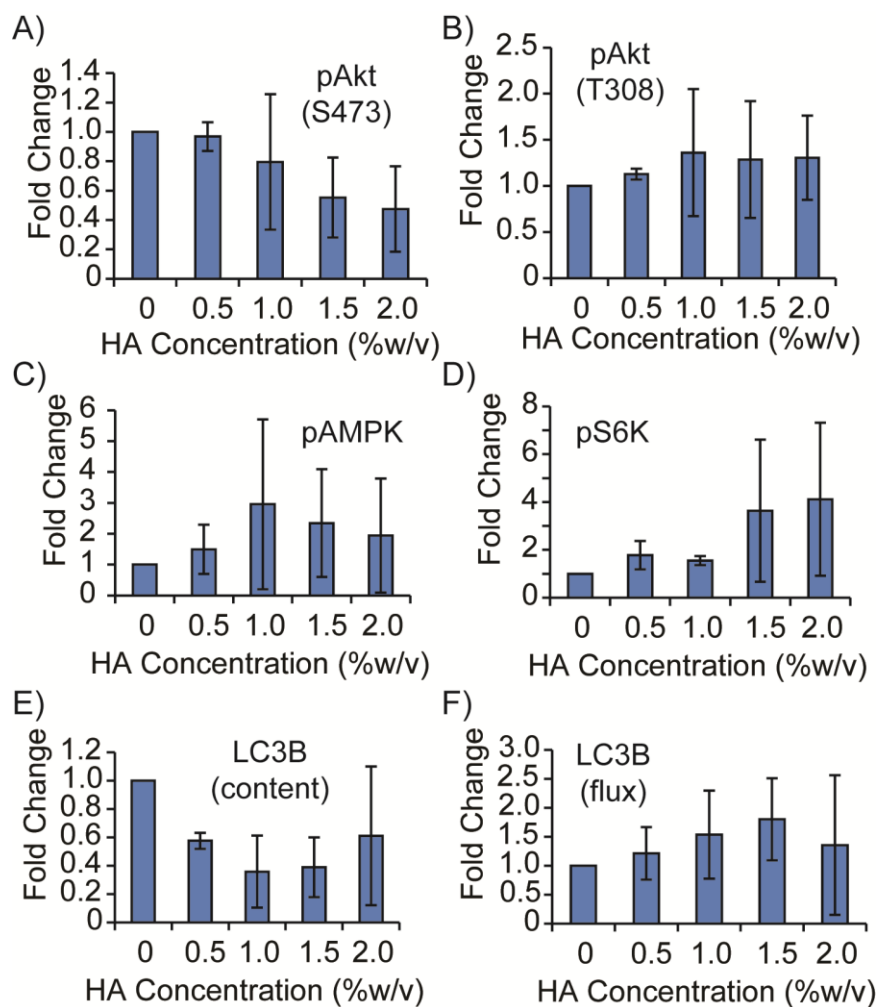
Supplemental Figure 8, LNCaP Western blot data. Densitometry analysis of Western blots for probed proteins involved in the AMPK-Akt-mTOR protein network. Error bars show standard deviation. Data was normalized to the control (cells grown in standard monolayer with liquid cell culture medium) of each replicate and the ensemble data across all replicates were plotted together.
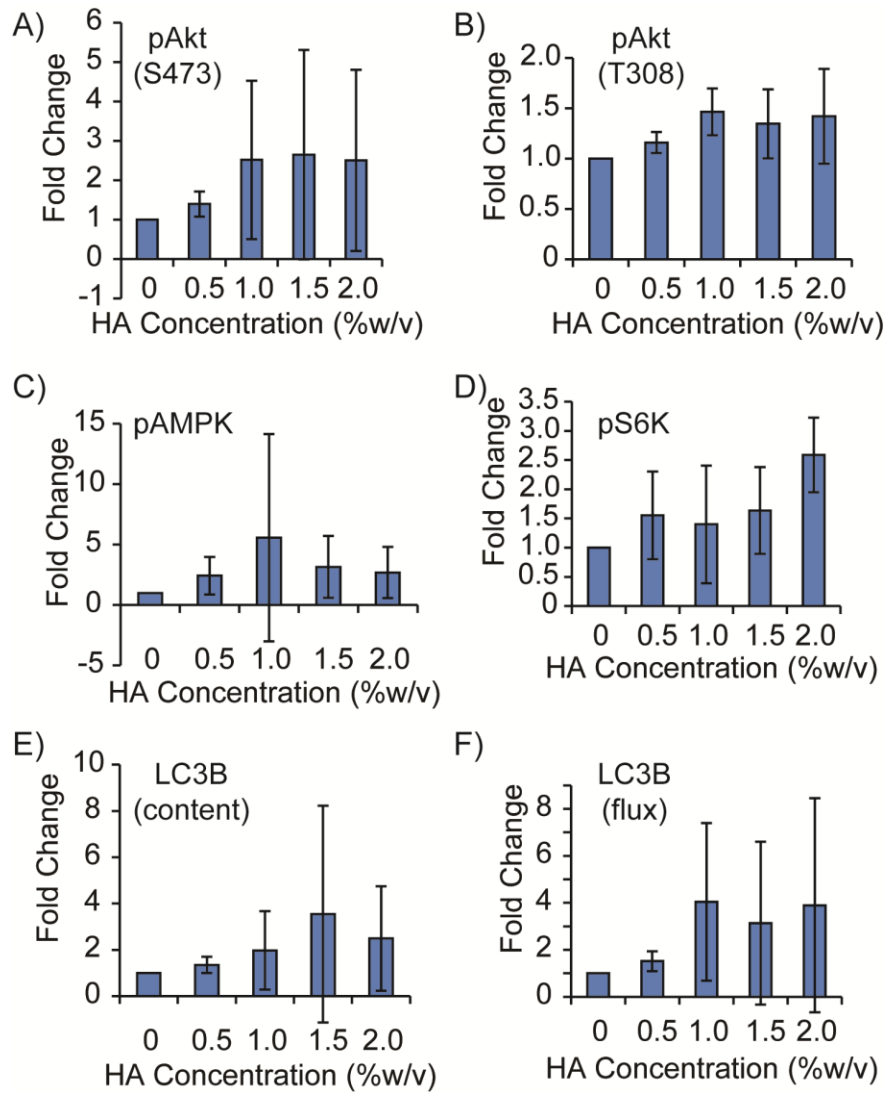
Supplemental Figure 9, PC3 Western blot data. Densitometry analysis of Western blots for probed proteins involved in the AMPK-Akt-mTOR protein network. Error bars show standard deviation. Data was normalized to the control (cells grown in standard monolayer with liquid cell culture medium) of each replicate and the ensemble data across all replicates were plotted together.
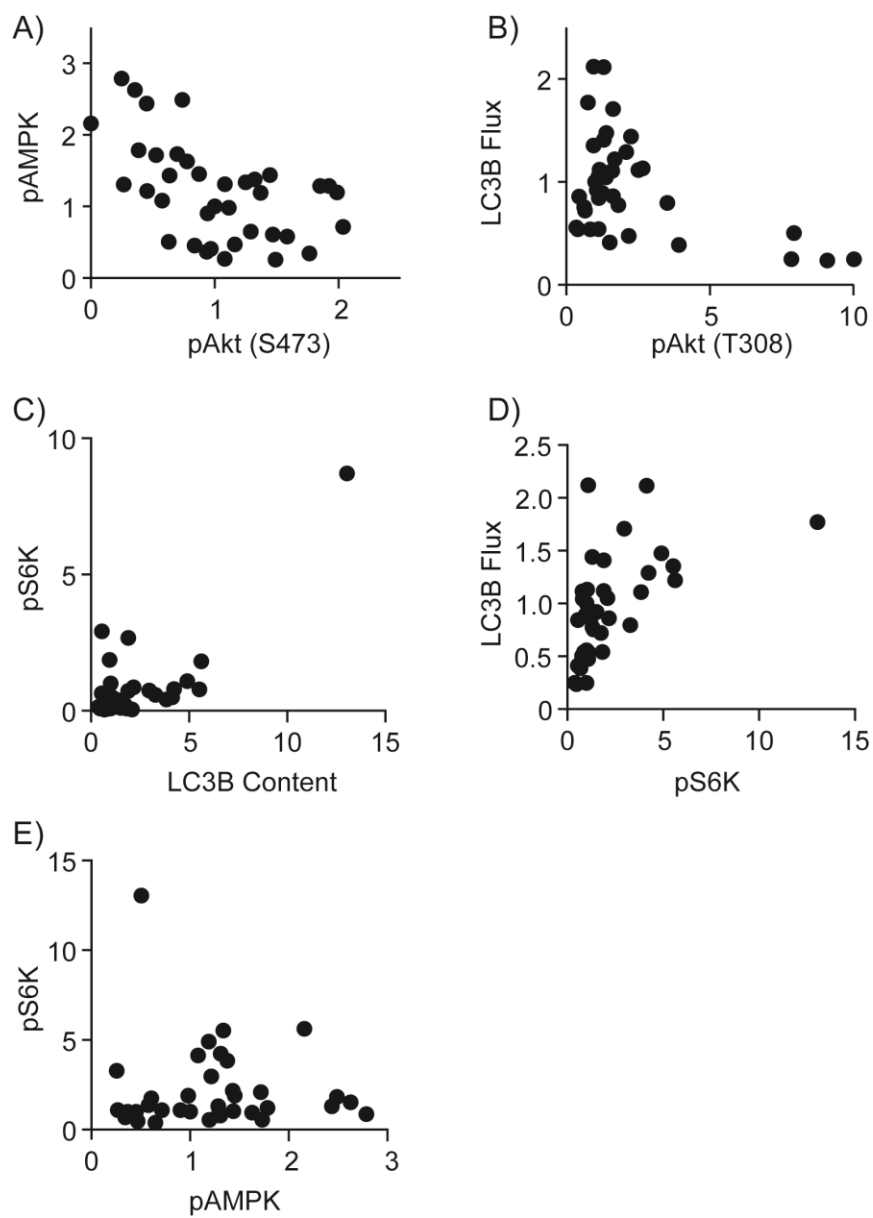
Supplemental Figure 10, Selected pairs of protein activation correlation datasets for LNCap cells. Statistically significant correlations were observed for A-D, based on Pearson's R (p<0.01). The full pairwise comparison is presented in the heat map in Figure 5.
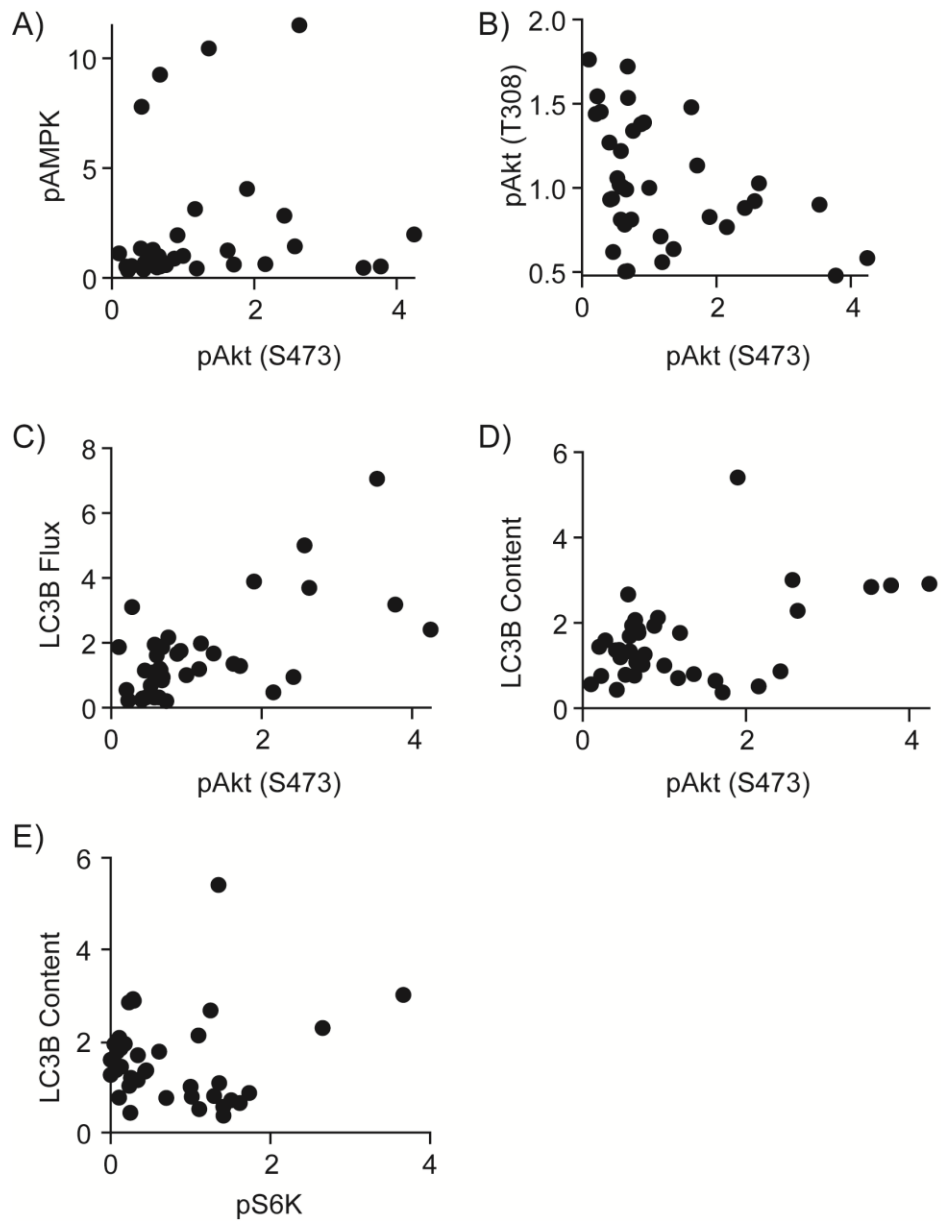
Supplemental Figure 11, Selected pairs of protein activation correlation datasets for PC3 cells.
Statistically significant correlations were observed for B-D, based on Pearson's R (p<0.01). The full
pairwise comparison is presented in the heat map in Figure 5.